Supplementary Information

Unraveling Structure-performance Relationship in Hard Carbon for Sodium-ion Battery by Coupling Key Structural Parameters

Chun Wu [abcd], Yunrui Yang [ac], Yifan Li [ac], Xiangxi He [ac], Yinghao Zhang [ac], Wenjie Huang [ac], Qinghang Chen [ac], Xiaohao Liu [ac], Shuangqiang Chen [ac], Qinfen Gu [e], Lin Li [ac], Sean C. Smith [f], Xin Tan *[ac], Yan Yu *[d], Xingqiao Wu *[ac], Shulei Chou *[ac]

a Institute for Carbon Neutralization Technology, College of Chemistry and Materials Engineering, Wenzhou University, Wenzhou, Zhejiang 325035, China

b College of Materials Science and Engineering, Changsha University of Science and Technology, Changsha 410114, China

c Wenzhou Key Laboratory of Sodium-Ion Batteries, Wenzhou University Technology Innovation Institute for Carbon Neutralization, Wenzhou, Zhejiang 325035, China

d Hefei National Research Center for Physical Sciences at the Microscale, Department of Materials Science and Engineering, CAS Key Laboratory of Materials for Energy Conversion, University of Science and Technology of China, Hefei, Anhui, 230026, China

e Australian Synchrotron (ANSTO), 800 Blackburn Road, Clayton, VIC 3168, Australia

f Integrated Materials Design Laboratory, Department of Materials Physics, Research School of Physics, Australian National University, Canberra, ACT 2601, Australia

E-mail: xintan@wzu.edu.cn (X. Tan), yanyumse@ustc.edu.cn (Y. Yu), xingqiaowu@wzu.edu.cn (X. Wu), chou@wzu.edu.cn (S.-L. Chou)

Experimental Section

Computational Methods

All density functional theory calculations were performed using the first-principles calculation software DS-PAW under the Device Studio platform. [1] Which uses the plane wave basis and the projector augmented wave (PAW), [2-4] it is used for treating core electrons. The Perdew, Burke, and Ernzerh of exchange-correlation functional within a generalized gradient approximation (GGA-PBE), [5] was used in our calculations, and the van der Waals (vdW) correction proposed by Grimme (DFT-D3) A constructed AB-stacked flat defect-free 6×6 supercell bilayer carbon structure was created, [6] with the model's lattice constants in the ab plane being 12.78Å and 14.76Å, respectively. To avoid interactions between periodic images, a vacuum layer of 18Å was set in the z direction. Then, by reducing the lattice constants to apply curvature, defects were introduced by removing some carbon atoms. C=O (carbonyl) were added, and the edges of the defects were passivated with hydrogen atoms. In all calculations, a cutoff energy of 500 eV was used, and Brillouin zone integrations were performed on a (3×3×1) Monkhorst-Pack k-point grid. All structures were relaxed until the residual atomic force was less than 0.03eV/Å, with total energy converging to within 10^{-5} eV.

The adsorption energy (E_{ads}) is defined as:

$$E_{ads}=E_{CNa}-E_{C}-E_{Na} \quad (1)$$

where E_{CNa} represents the total energy after inserting Na, E_C represents the substrate energy before inserting Na, and E_{Na} represents the energy of an individual Na atom.

Synthesis of hard carbons and electrodes

The typical preparation process of the hard carbons were as following steps: First, grinded the bamboo (purchased from Ji'an city, Jiangxi Province) into powder and stirred with 6.0 M HCl solution for 6 h, then washed with distilled water until pH reached 7. Second, after drying at a temperature of 90 ^{o}C for 12 h, the powder was

pre-oxidized under 275, 325, 375 ^{o}C at 5 ^{o}C/min in the tubular furnace for 1 h under O_2/N_2 atmosphere. After cooled down to the room temperature, the as-obtained sample were named as AL, AM and AH. Third, put the as-prepared AL, AM and AH samples in the tubular furnace and carbonized at 1400 ^{o}C for 3 h under N_2 atmosphere with the heating rate about 5 ^{o}C/min, the resultant material were donated as HC-AL, HC-AM and HC-AH. For comparison, the acid-treated bamboo powder under pre-carbonization under 275 ^{o}C at 5 ^{o}C/min under N_2 atmosphere for 1 h was named as NL, and the NL material carbonized at 1400 ^{o}C under N_2 atmosphere for 3 h was named as HC.

Preparation procedure of the active electrode can be described as following steps : First, weigh the as-prepared hard carbon samples, super P and sodium alginate with the ratio about 8: 1: 1, and added appropriate amount of distilled water. Then, mixture was vibration stirred for 0.5 h. After homogeneously mixed, slurry was scraped on the aluminum foil, and put it in drying oven, after dried at 90 ℃ for 12 h, the anode can be obtained with diameter about 1.0 cm, the active mass loading is about 1.2-1.4 mg cm^{-2}. The similar preparation process can be applied for Prussian blue (PB) electrode with the ratio about 8: 1: 1 for active material, super P and sodium alginate (the active mass loading is about 8.4-8.6 mg cm^{-2}), oxides and polyanion electrode were prepared under the ratio about 7: 2: 1 for active material, super P and polyvinylidene fluoride (the active mass loading is about 4.8-5.0 mg cm^{-2} for oxide electrode and 2.8-3.0 mg cm^{-2} for polyanion electrode).

Materials characterization

The morphology and crystal structure of the as-prepared materials were observed by scanning electron microscopy (SEM) and transmission electron microscopy (HRTEM; FEI Tecnai F20). The structure of the as-prepared materials were measured by X-ray diffraction (XRD, X'pert18 powder D/MAX2500V and Rigaku Smart Lab with the Cu Kα radiation, set at the operating voltage of 40 kV (λ = 0.154 nm)), and Raman spectra were recorded with a Renishaw inVia instrument equipped with a 532 nm wavelength laser. Fourier transform infrared (FTIR) spectra were recorded on a

Thermo Scientific Nicolet iS20 FTIR. The SSA, total pore volume and pore size distribution of the hard carbon samples were measured through Quantachromeautosorb automated gas sorption system via N_2 sorption methods and CO_2 adsorption/desorption isotherms at 273 K on a Micromeritics ASAP2460 analyser. SAXS were measured by Xeuss 2.0 (France), sample test distance: 2480mm (SAXS). The chemical elemental composition of the resultant electrode materials were investigated by by a ESCALAB 250xi X-Ray Photoelectron Spectroscopy (XPS). PDF measurements were performed using a beam energy of 21 keV. This configuration facilitated the collection of high-resolution diffraction data, which was utilized to analyze the crystal structure, phase composition, and microstructural properties of the samples. The data covered a Q range up to 18.5 $Å^{-1}$. The sample was contained in a 1.0 mm glass capillary for measurement.

The layer stacking distance (*Lc*) and the longitudinal size of structural elements (*La*) were calculated based on the following formula (Scherrer equation):

$$Lc\&La=k\lambda/(\beta cos\theta) \qquad (2)$$

Where, k presents scherrer constant (k = 0.9 for *Lc* and k = 1.84 for *La*), λ stands for the radiation wavelength, β is the half-height width of the (002) reflection, θ presents the reflection angle of (002) or (100). The number of layers in a stack was calculated according to the following formula:

$$n=(Lc/d_{002})+1 \qquad (3)$$

Electrochemical measurements

Electrochemical behavior measurements were explored through button battery cells (CR2032) with glass fiber (GF/A, Whatman, UK) as the separators, sodium electrode as the counter electrodes with a thickness of 0.1 mm and diameter of 1.2 cm, and 1 M $NaPF_6$ in EC/DMC (v/v=1: 1) and 1 M $NaPF_6$ in DEGDME as electrolyte. And electrolyte for cathodes were NTE-0002 (which was purchased from Wenzhou NaTech New Energy Technology Co., Ltd). The amount of electrolyte used for the button battery cells are about 100 μL. All cells were fabricated within an argon-filled glovebox, maintaining H_2O and O_2 levels below 0.01 ppm. Galvanostatic charge and

discharge measurement for hard carbon, PB, oxides and polyanion electrodes were performed by NEWARE battery testing system under the potential range of 0-2 V, 2-3.8V, 2-4 V and 2.8-3.8 V. Electrochemical workstation (CHI760E) was used for cyclic voltammetry (CV) at 0.1, 0.2, 0.5 and 1mV s^{-1} under 0 to 2.0 V. The current density for cycle test in ester-based electrolyte was 20 mA g^{-1} for two cycles and then 50 mA g^{-1} for long-term measurement. While, the current density for cycle test in ether-based electrolyte was 100 mA g^{-1} after 20 mA g^{-1} for the first two cycles. Current density for low-temperature cycle test was 20 mA g^{-1}. Land battery system was utilized for Galvanostatic intermittent titration technique (GITT) measurement and steps are as follows: (1) 10min constant current discharge at 20 mA g^{-1} current density; (2) Set aside for 1.5 h; (3) If the voltage after the battery is set aside is greater than 0 V, return to step 1; if the voltage after the battery is set aside is less than 0V, proceed to the next step (4) Charge at constant current for 10 min at 20 mA g^{-1} current density; (5) Set aside for 1.5 h; (6) If the voltage after the battery is set aside is less than 2 V, return to step 1; if the voltage after the battery is set aside is greater than 2 V, stop the test.

In addition, the electrolyte in coin full cell was NTE-0002 and 1 M $NaPF_6$ in DEGDME under voltage range 1.6 - 3.8 V, and tested under 0.1 C for the first cycle and 1.0 C for the long-tern charge/discharge measurement. The voltage range for soft package battery was 1.5 - 3.7 V, and tested under 0.1 C for the first cycle and 0.5 C for the long-tern measurement by constant current/constant voltage charge and constant current discharge test method. 2.0 - 3.6 V was applied for voltage range of cylindrical battery measurement, and tested under 0.1 C for the five cycles and 0.5 C for the long-tern measurement with constant current charge and discharge with low current charge and high current discharge method for the rate performance. All the electrochemical measurements were conducted at 25 ^{o}C.

Calculation of apparent Na^+ chemical diffusion coefficients through GITT results.

The principle of constant current intermittent titration test is to apply a constant

current to the measuring electrode for a period of charging and discharging under specific conditions, and then stop applying current, and observe potential change of electrode with time during the applied current period and the final equilibrium voltage. Thus, the relaxation behavior of the electrode reaction potential can be discerned through the study of potential variations over time, the reaction kinetics can be further inferred and calculated. The calculation formula is as follows.

$$D=(4/\pi\tau)(m_B V_M/M_B S)^2(\Delta E_S/\Delta E\tau)^2 \quad (4)$$

where τ presents current pulse time; m_B is mass of active material from the electrode; V_M represents molar volume of the material; M_B stands for molar mass of the material; M_B/V_M shows density of the hard carbon material; S presents geometric area of the electrode sheet; $\Delta E\tau$ and ΔE_S can be obtained from GITT curves, where ΔE_S stands for the difference between the potential after the current is applied and relaxation stabilized and $\Delta E\tau$ refers to the value of the change in electrode potential after applying a current for a period of time other than the voltage drop portion.

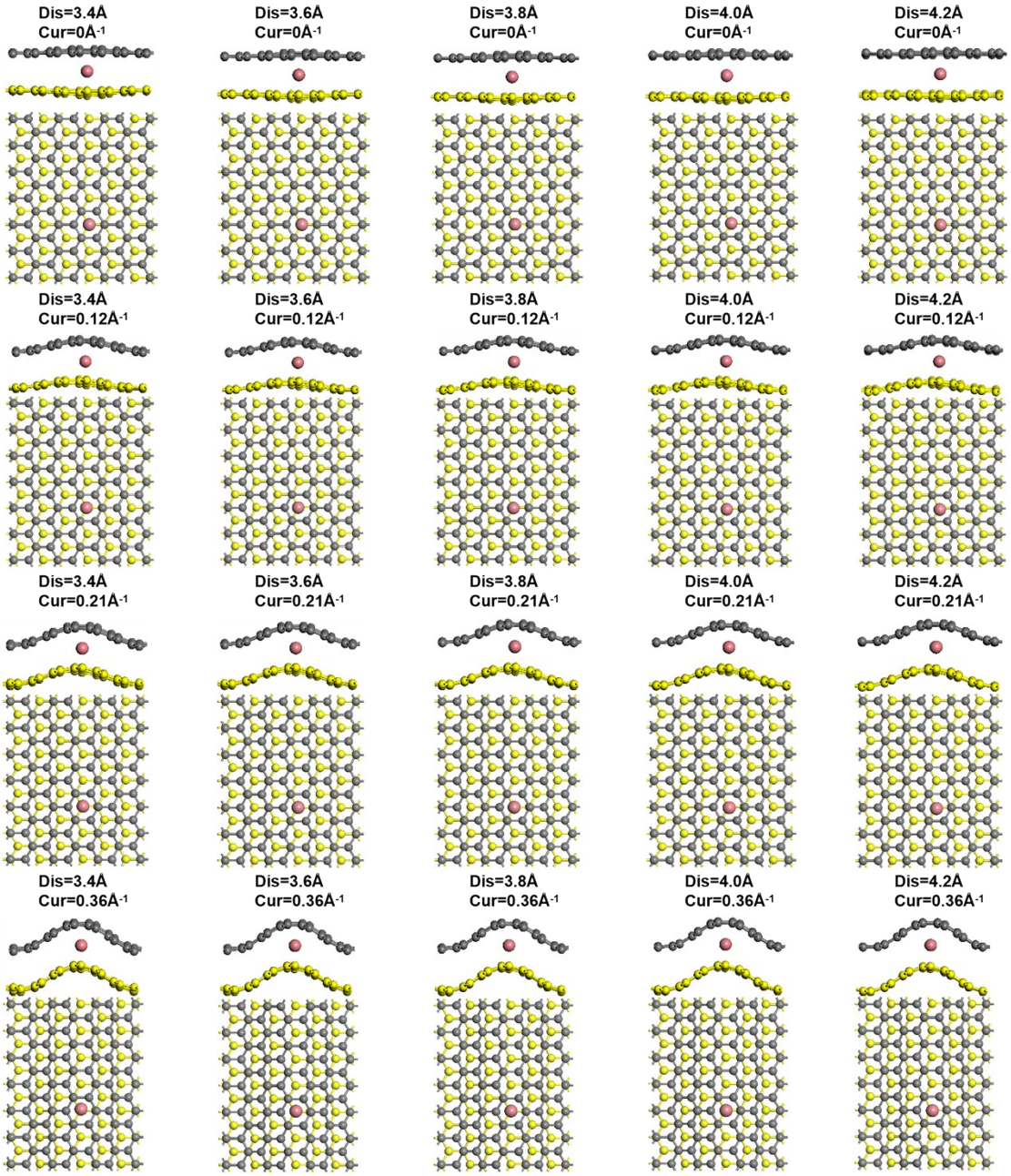

Fig. S1 Top view and side view of different layer spacings of defect-free bilayer graphene under various curvatures.

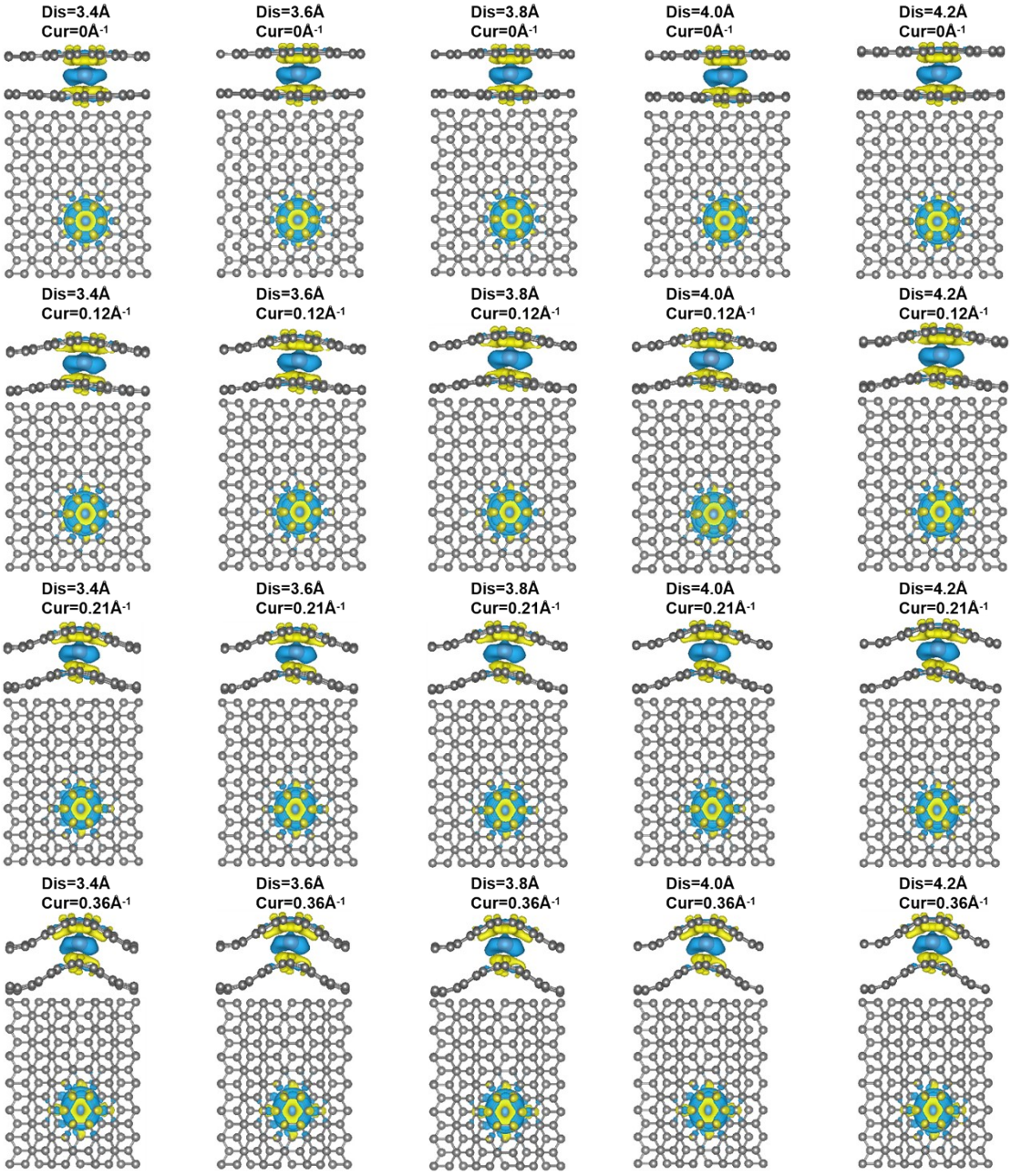

Fig. S2 Top view and side view of the differential charge density distribution of defect-free bilayer graphene at different layer spacings under various curvatures.

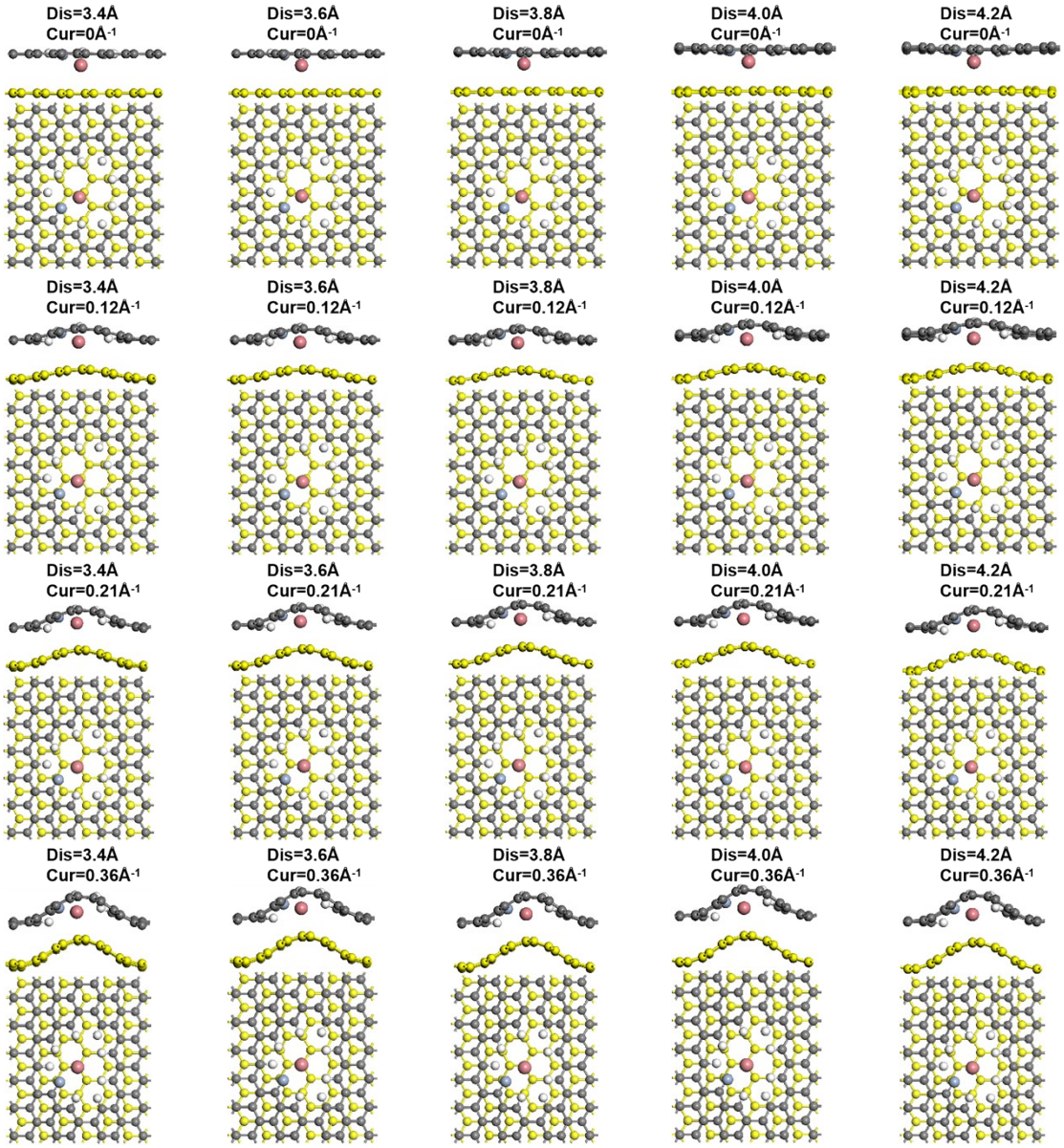

Fig. S3 Top view and side view of different layer spacings of O-defective bilayer graphene under various curvatures.

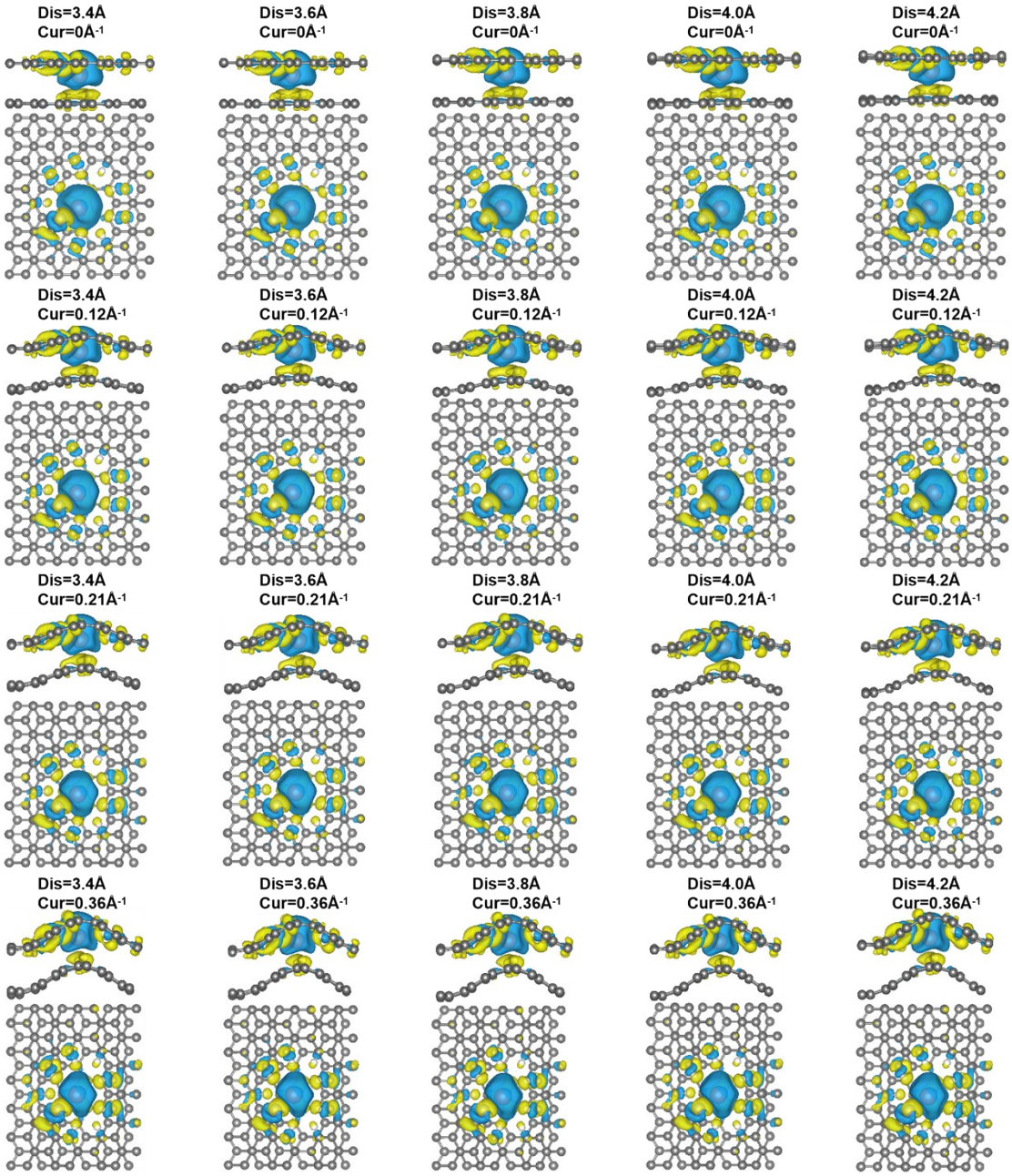

Fig.S4 Top view and side view of the differential charge density distribution of O-defective bilayer graphene at different layer spacings under various curvatures.

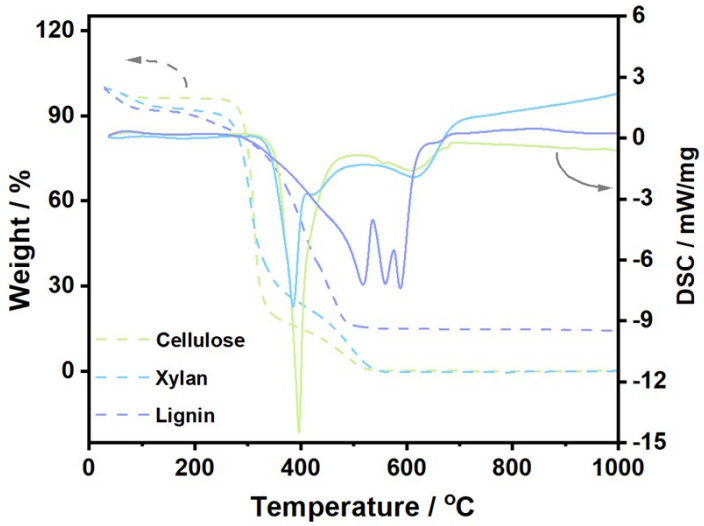

Fig. S5 The TG and DSC curves of cellulose, xylan and lignin.

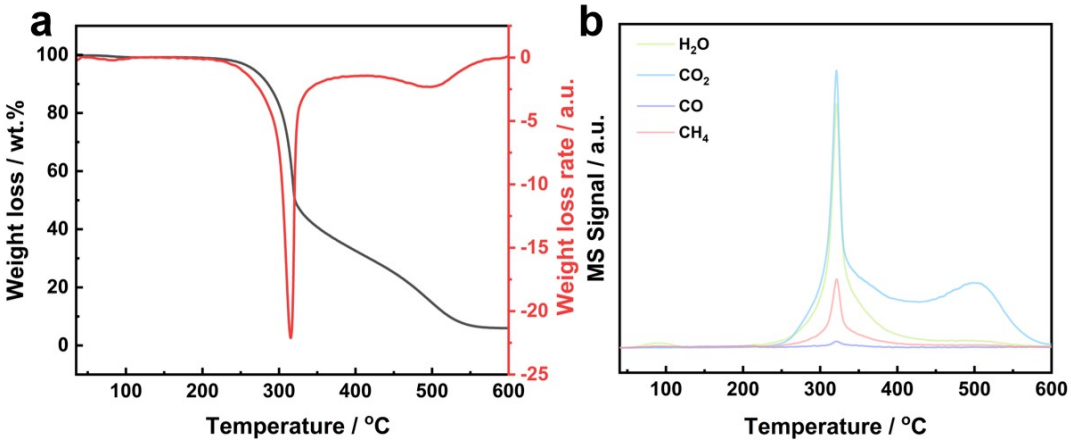

Fig. S6 TG-MS curves of the acid-treated bamboo.

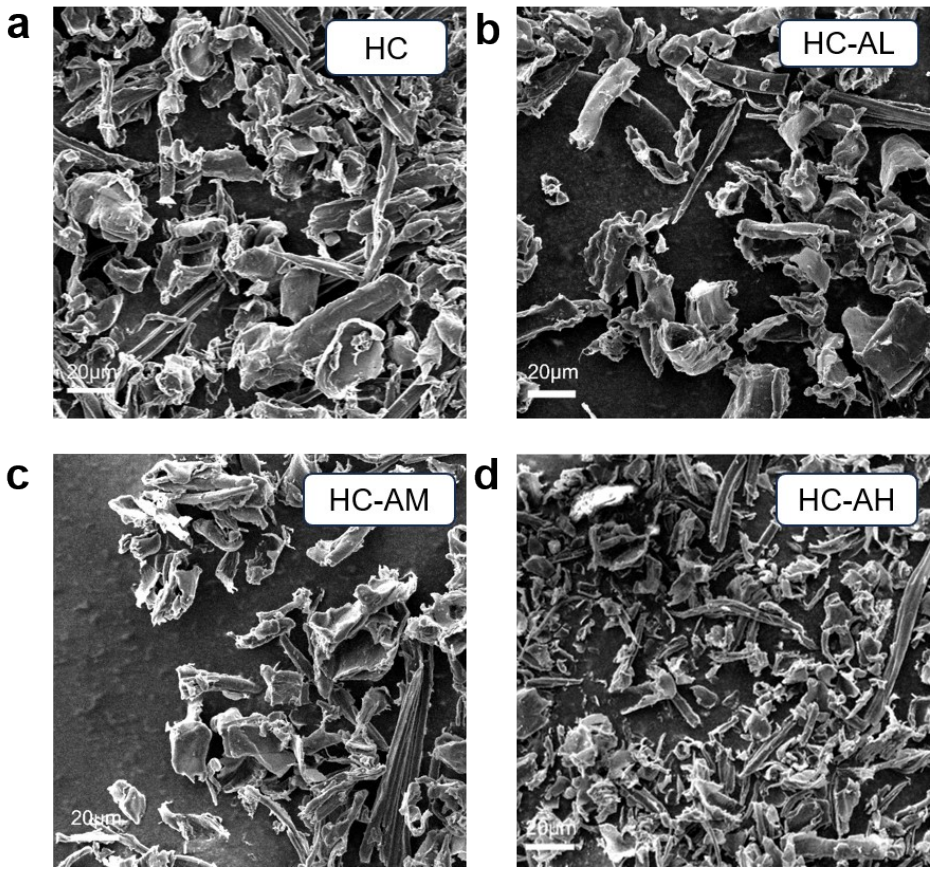

Fig. S7 SEM images of the (a) HC, (b) HC-AL, (c) HC-AM and (d) HC-AH.

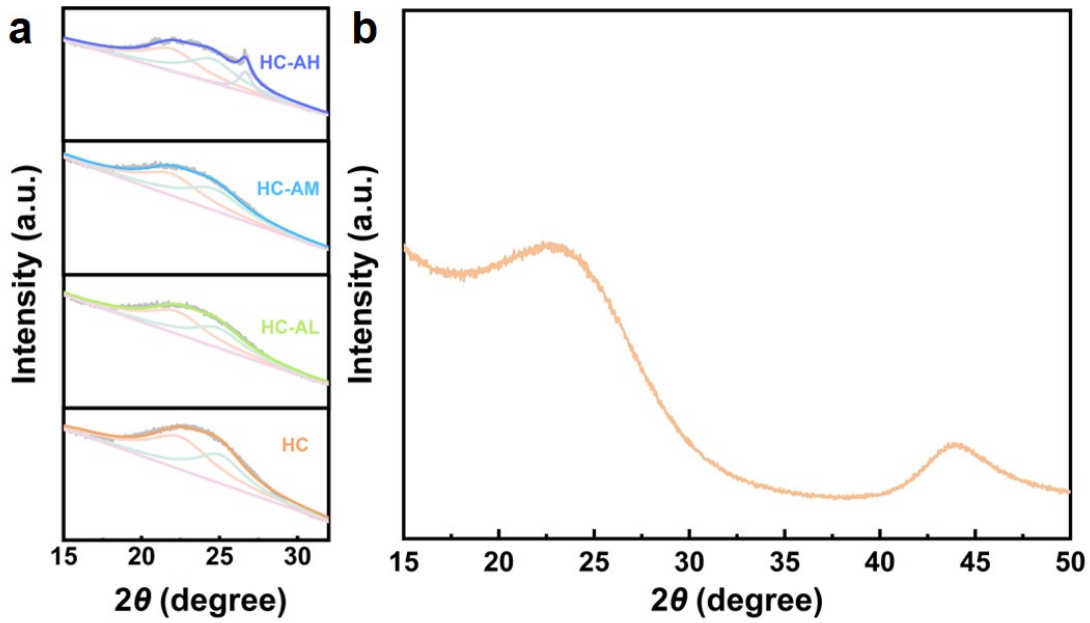

Fig. S8 (a) Curves after peak fitting of d_{002} peak of XRD pattern of HC, HC-AL, HC-AM, HC-AH, (b) XRD pattern of HC.

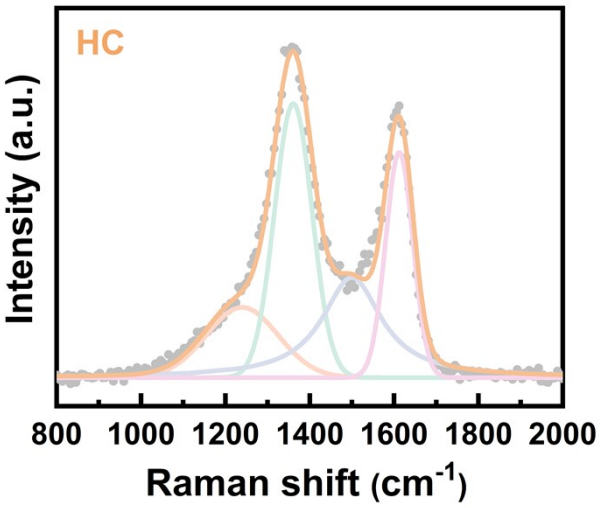

Fig. S9 Raman pattern of HC.

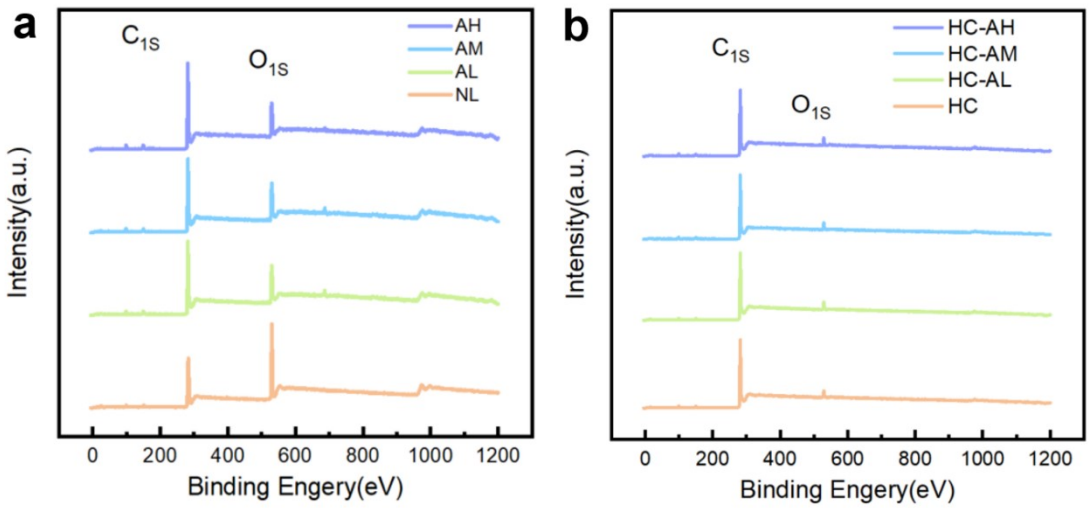

Fig. S10 (a) XPS pattern of NL, AL, AM and AH, (b) XPS pattern of HC, HC-AL, HC-AM and HC-AH.

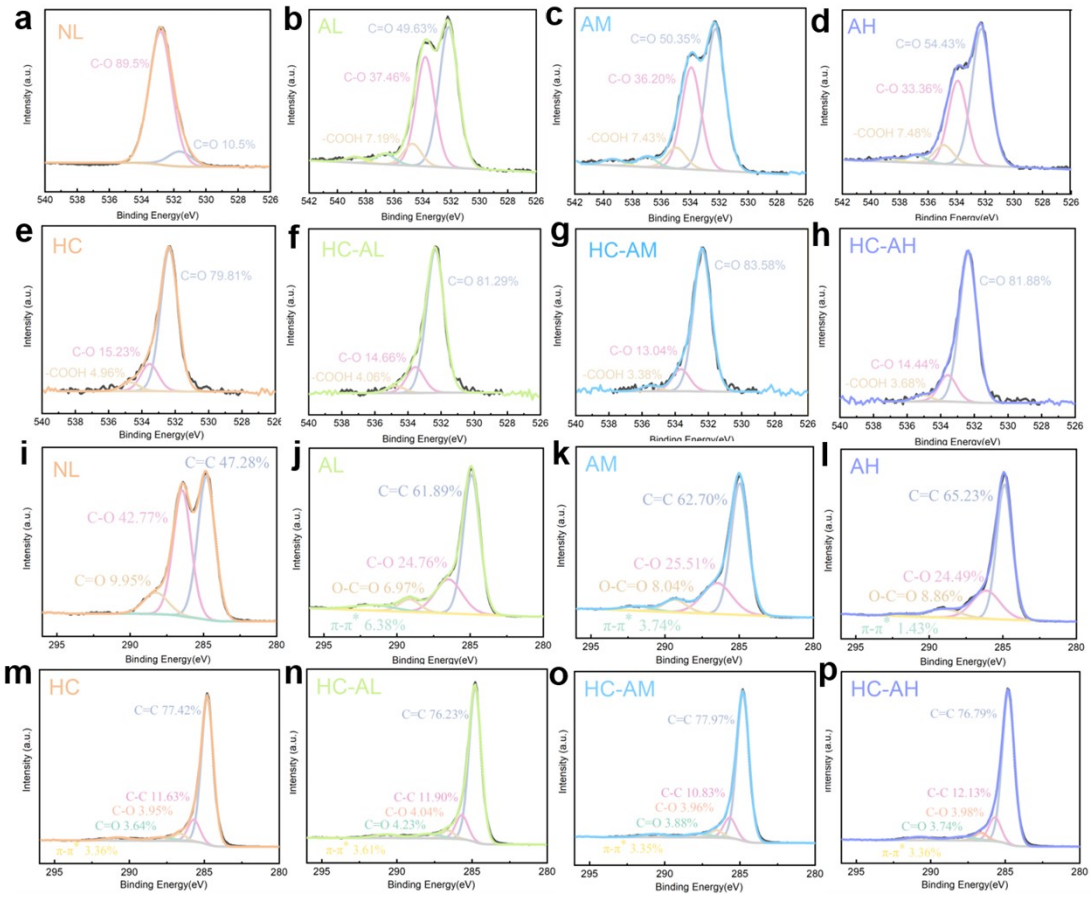

Fig. S11 (a-h) O1s fitting curve of NL, AL, AM, AH, HC, HC-AL, HC-AM, HC-AH, (i-p) C1s fitting curve of NL, AL, AM, AH, HC, HC-AL, HC-AM, HC-AH.

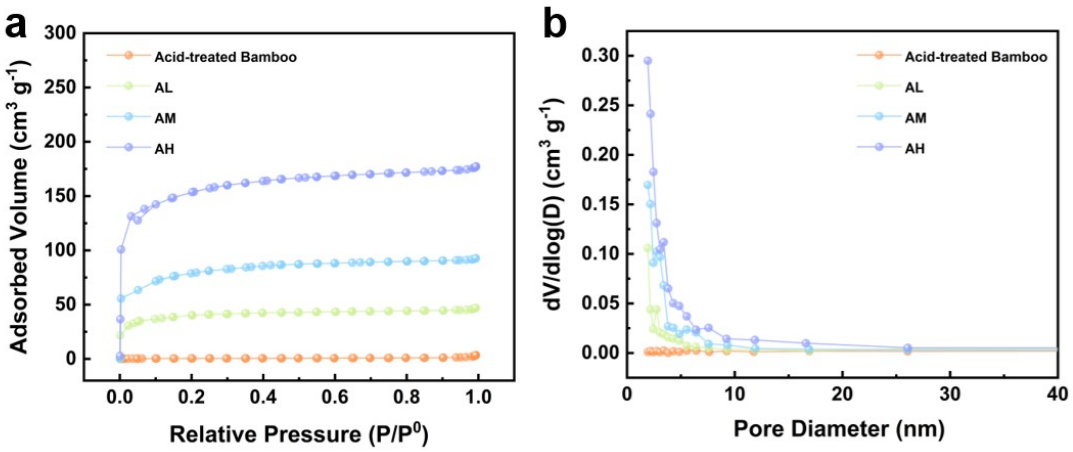

Fig. S12 (a) N_2 adsorption-desorption isotherms, (b) The corresponding pore size distributions of acid-treated bamboo, AL, AM and AH.

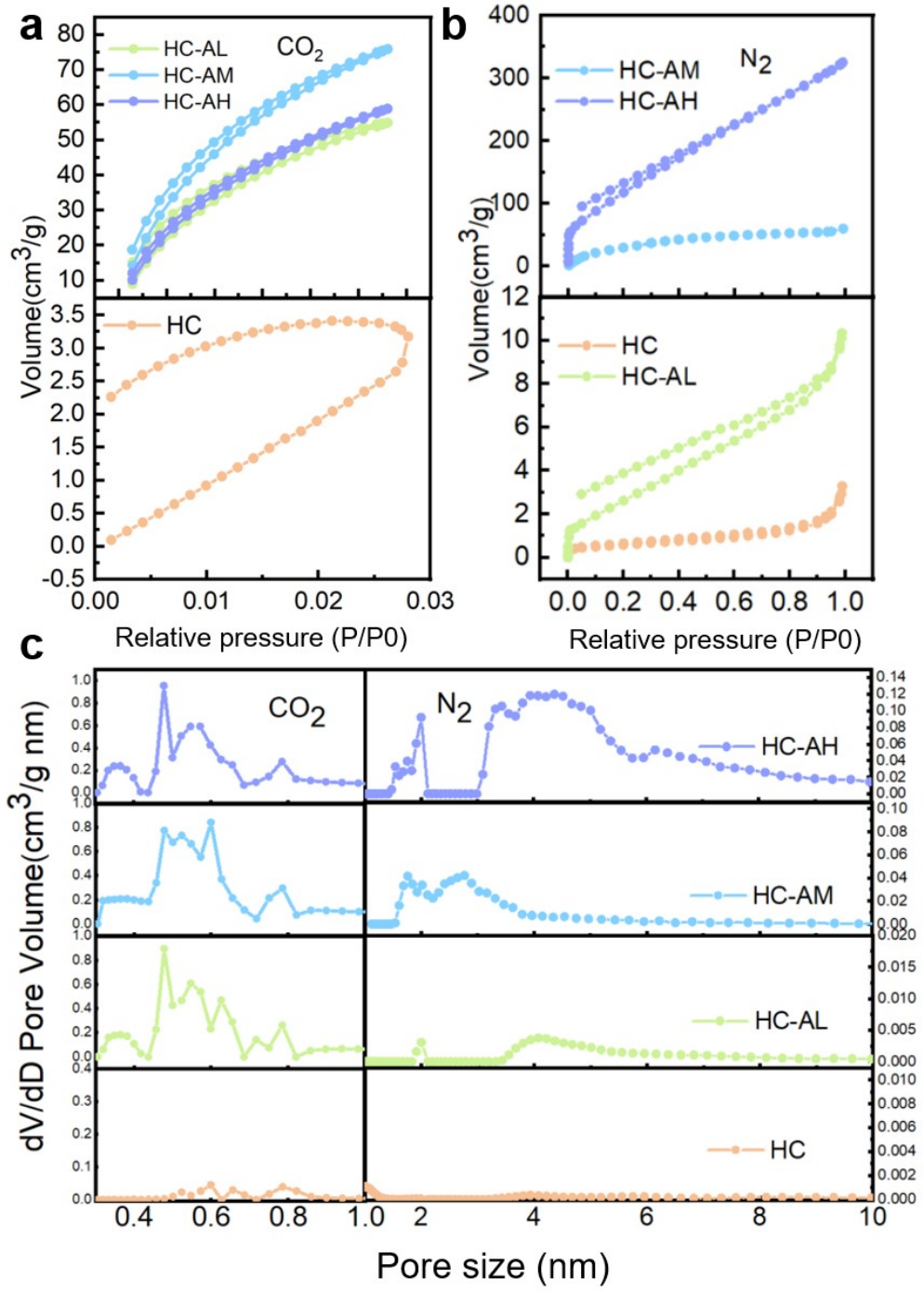

Fig. S13 (a, b) CO_2 and N_2 adsorption-desorption isotherms, (c) The corresponding pore size distributions of HC, HC-AL, HC-AM, HC-AH.

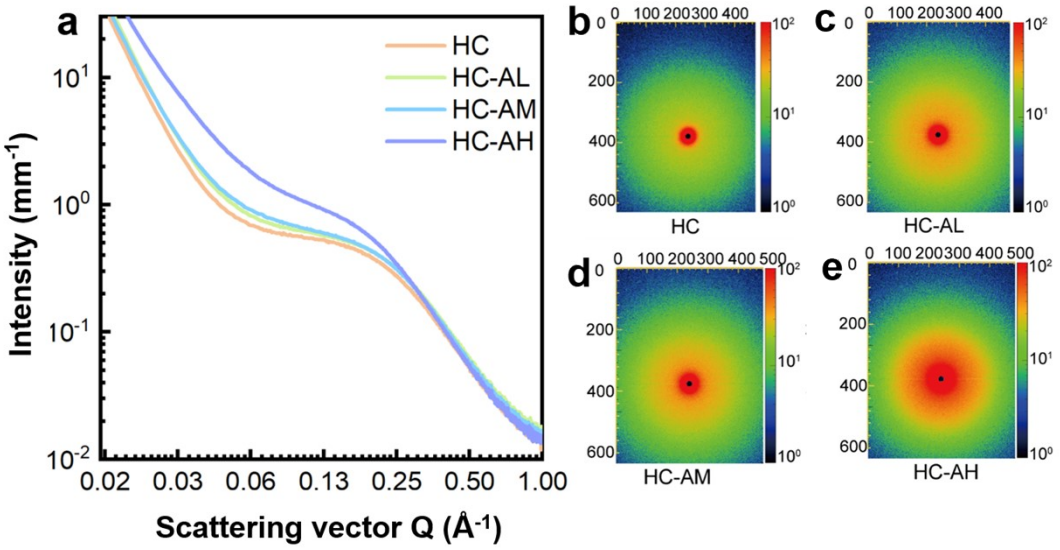

Fig. S14 (a) SAXS curves of HC, HC-AL, HC-AM and HC-AH, (b-e) Wide-angle diffraction patterns of HC, HC-AL, HC-AM and HC-AH.

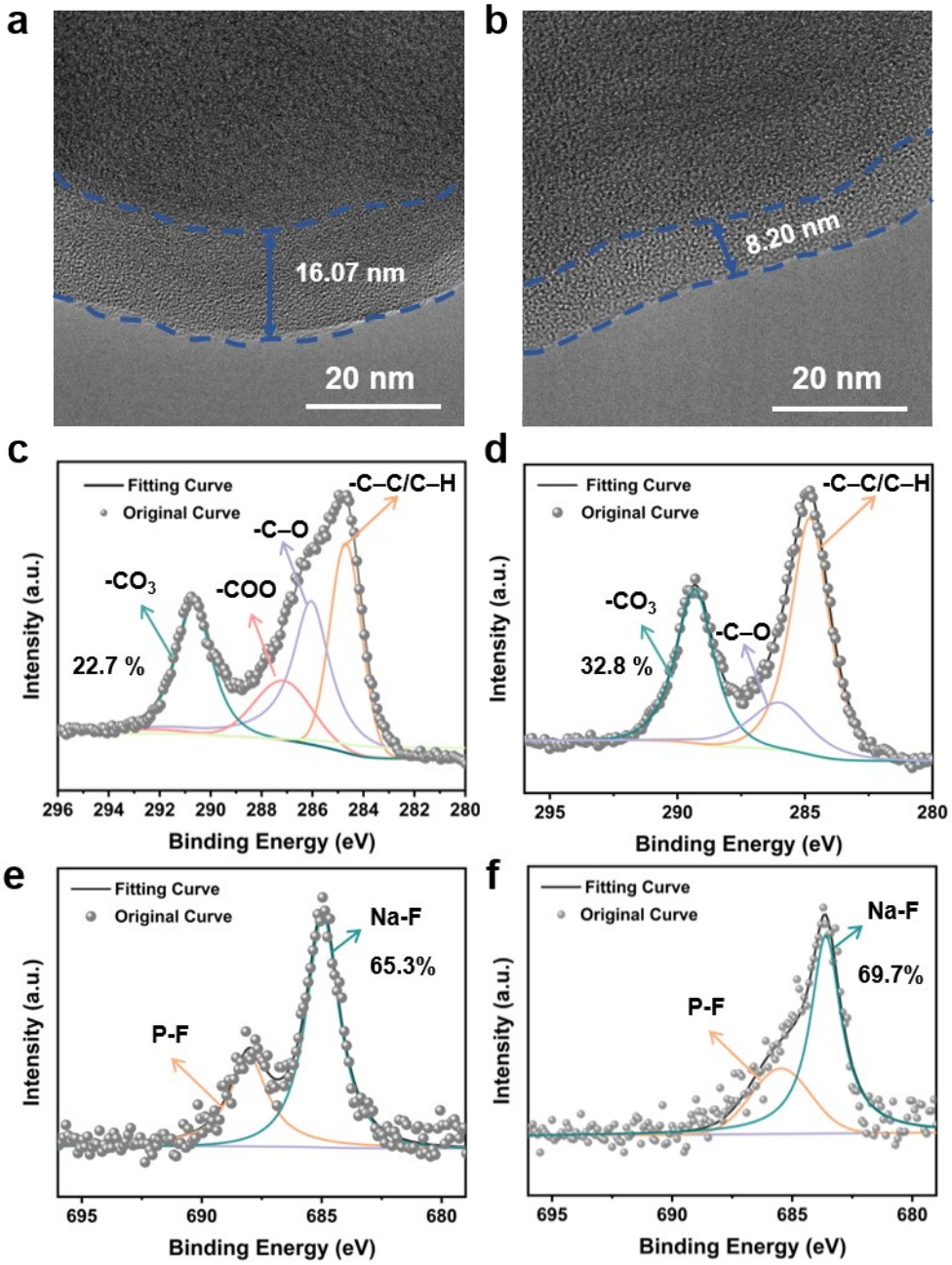

Fig. S15 HRTEM images of the SEI from HC-AL in (a) ester-based electrolyte and (b) ether-based electrolyte, XPS spectra of F1s and C1s from SEI on HC-AL in (c, e) ester-based electrolyte and (d, f) ether-based electrolyte

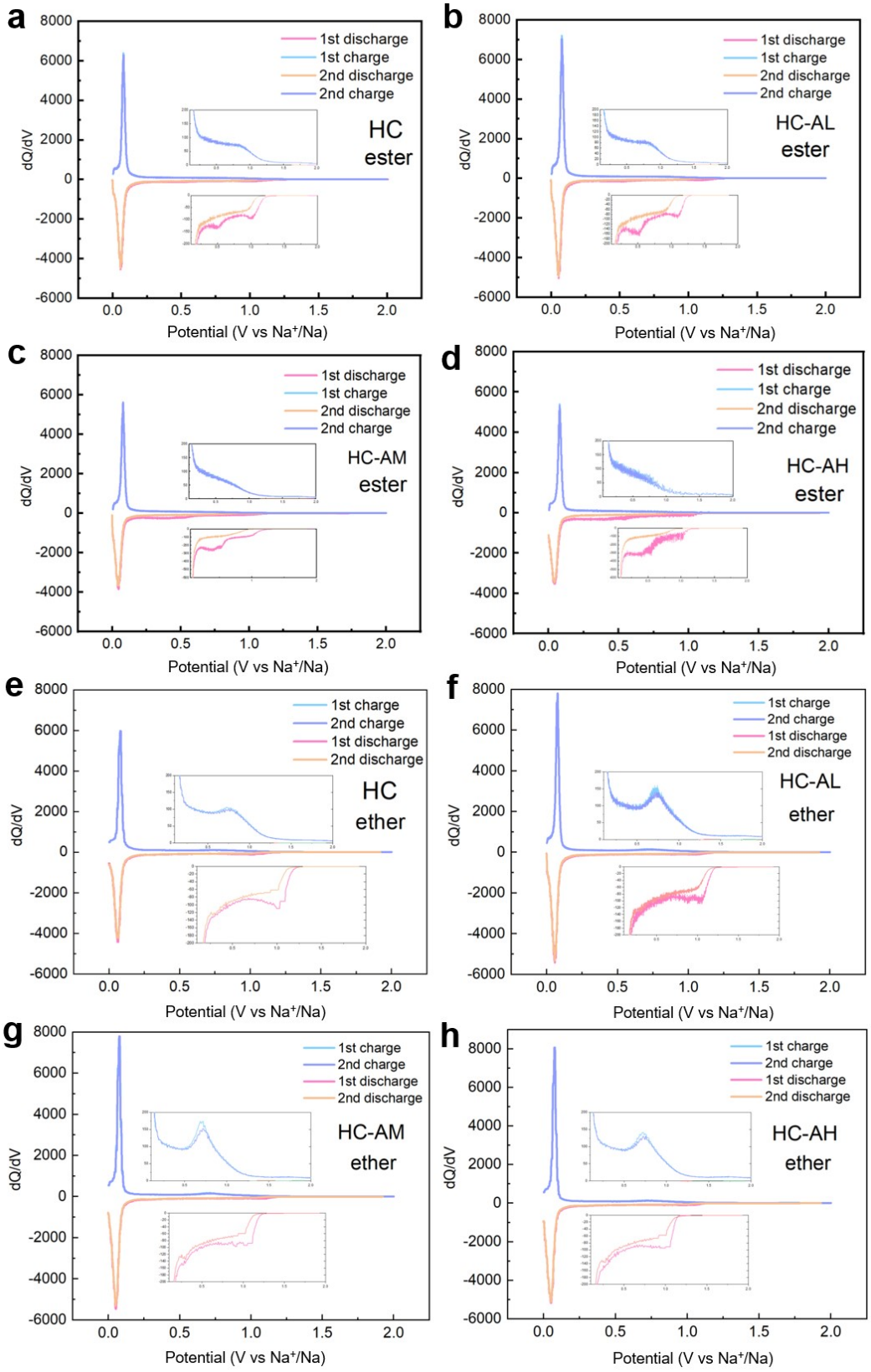

Fig. S16 *d*Q/*d*V calculated from the first and second charge/discharge curves in (a-d) ester-based electrolyte and (e-h) ether-based electrolyte of HC, HC-AL, HC-AM, HC-AH.

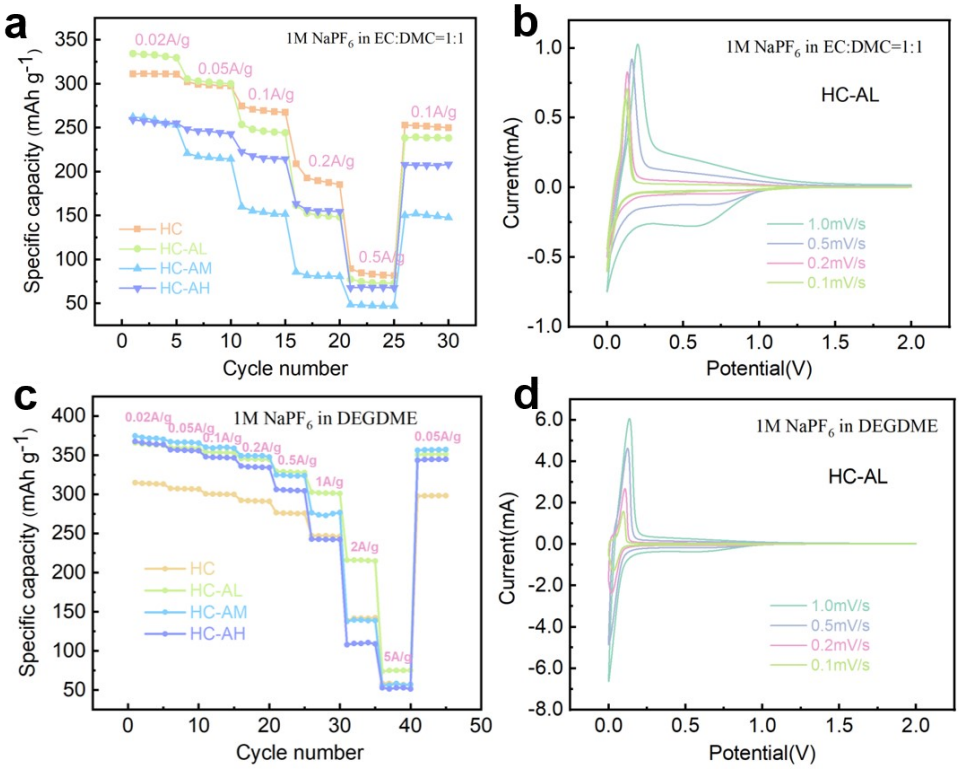

Fig. S17 Rate performance of different hard carbons in (a) ester-based electrolyte and (c) ether-based electrolyte and CV curves under different scan rates of HC-AL in (b) ester-based electrolyte and (d) ether-based electrolyte.

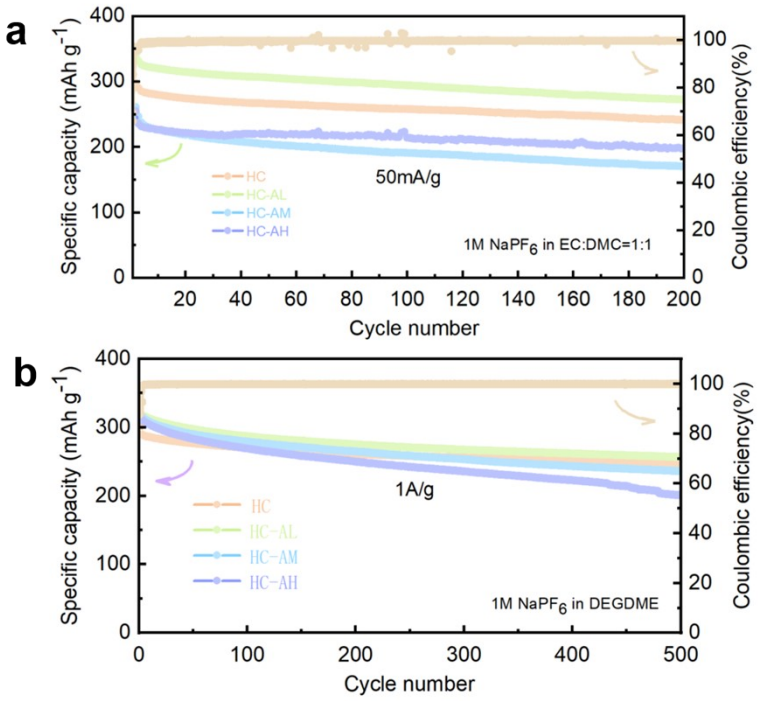

Fig. S18 Cycle performance of different hard carbons in (a) ester-based electrolyte and (b) ether-based electrolyte.

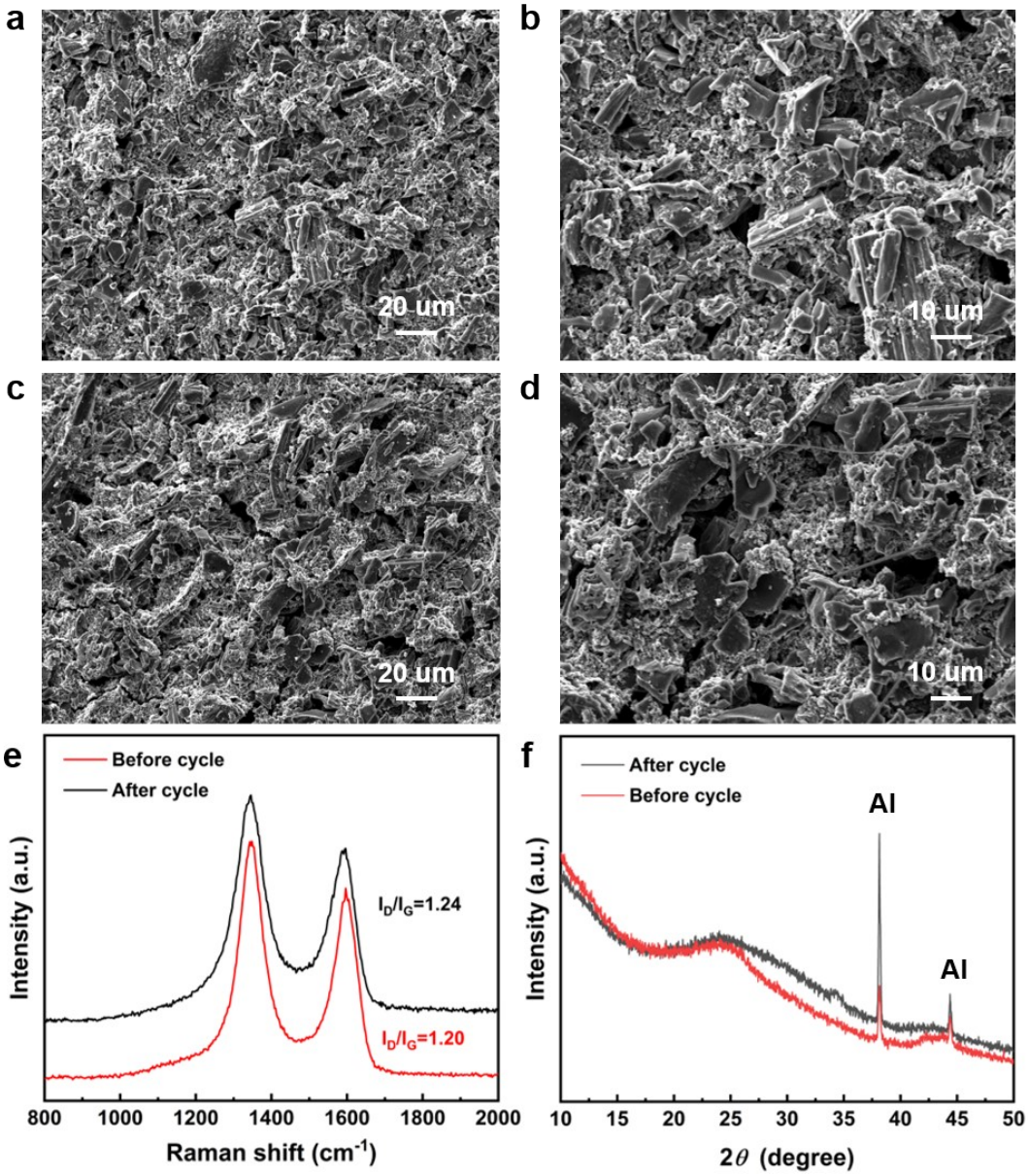

Fig. S19 SEM images (a-d), Raman (e) and XRD spectrum (f) of the HC-AL electrode in ether-based electrolyte before and after 500 cycles.

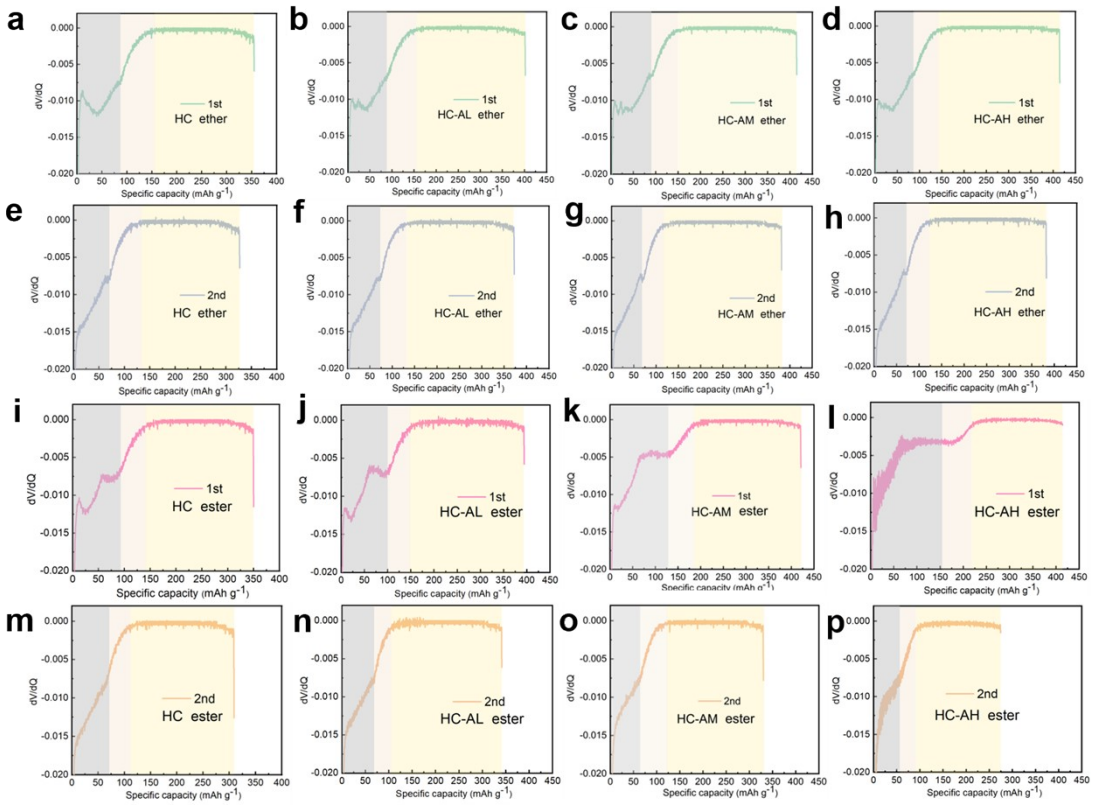

Fig. S20 (a-d) *d*V/*d*Q calculated from the first discharge curves in ether-based electrolyte of HC, HC-AL, HC-AM, HC-AH, (e-h) *d*V/*d*Q calculated from the second discharge curves in ether-based electrolyte of HC, HC-AL, HC-AM, HC-AH, (i-l) *d*V/*d*Q calculated from the first discharge curves in ester-based electrolyte of HC, HC-AL, HC-AM, HC-AH, (m-p) *d*V/*d*Q calculated from the second discharge curves in ester-based electrolyte of HC, HC-AL, HC-AM, HC-AH.

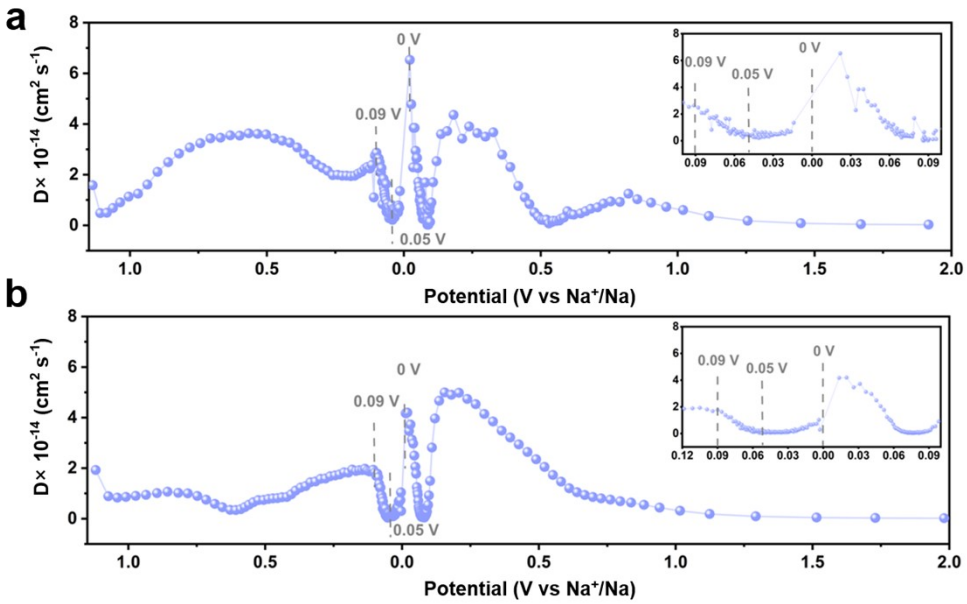

Fig. S21 GITT curves of HC-AL in (a) ether-based electrolyte and (b) ester-based electrolyte.

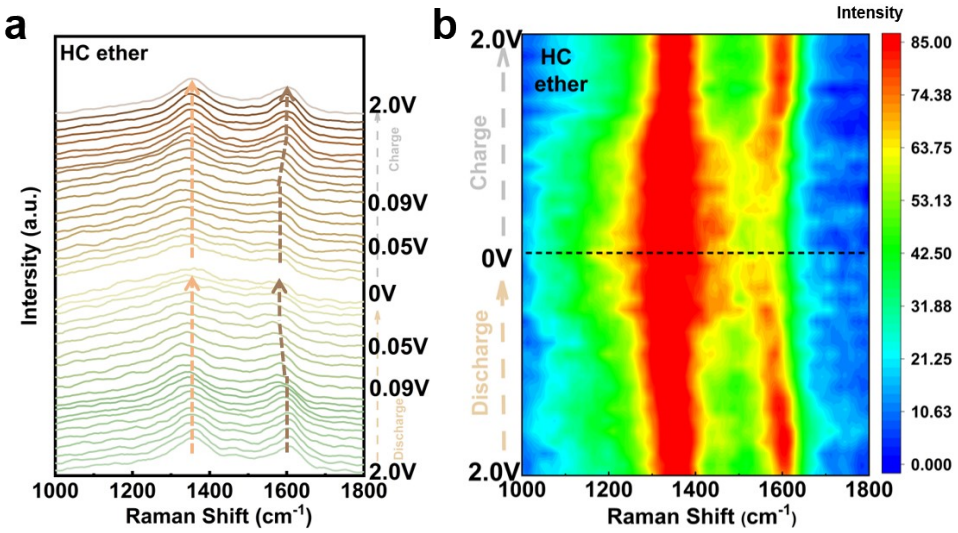

Fig. S22 (a-b) *In-situ* Raman spectra of HC in ether-based electrolyte.

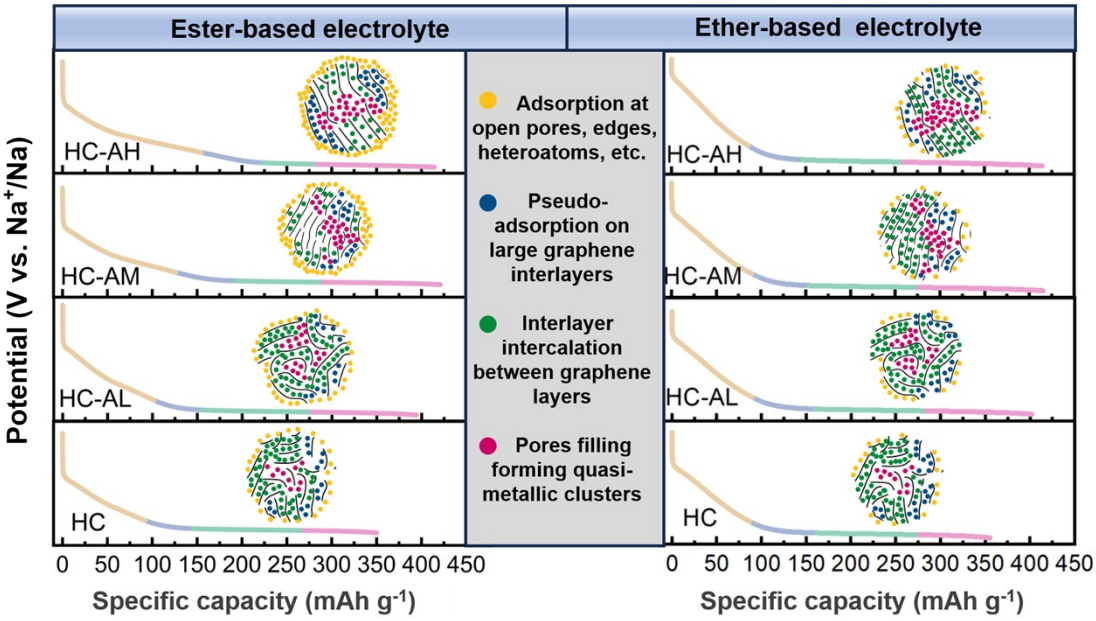

Fig. S23 Schematic diagram for sodium storage stages of HC-AH, HC-AM, HC-AL and HC in ester-based and ether-based electrolyte.

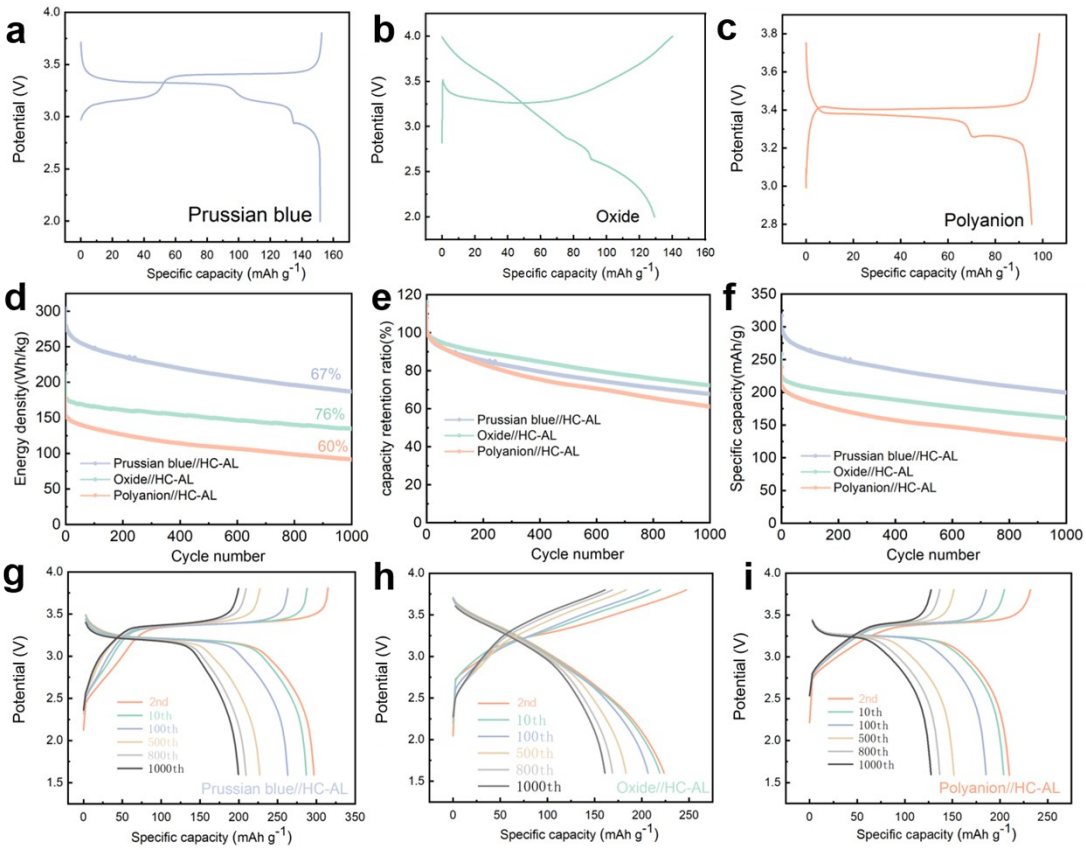

Fig. S24 (a-c) The first charge/discharge curves of three cathodes at 0.1 C, (d-f) Cycle stability of Prussian blue//HC-AL, Oxide//HC-AL and polyanion//HC-AL, (g-i) The charge/discharge curves of different full-cell under various cycles.

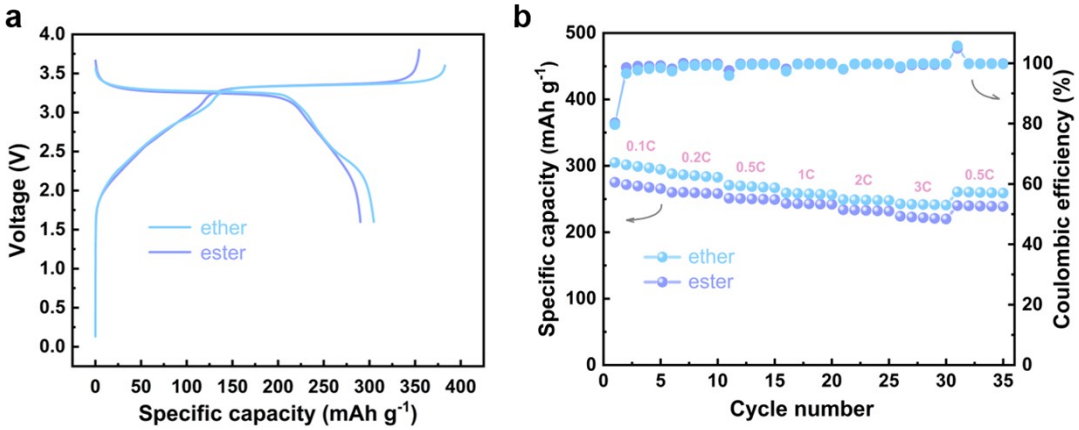

Fig. S25 Comparison of first (a) charge/discharge curves and (b) rate performance of Prussian blue//HC-AL in ester-based and ether-based electrolyte.

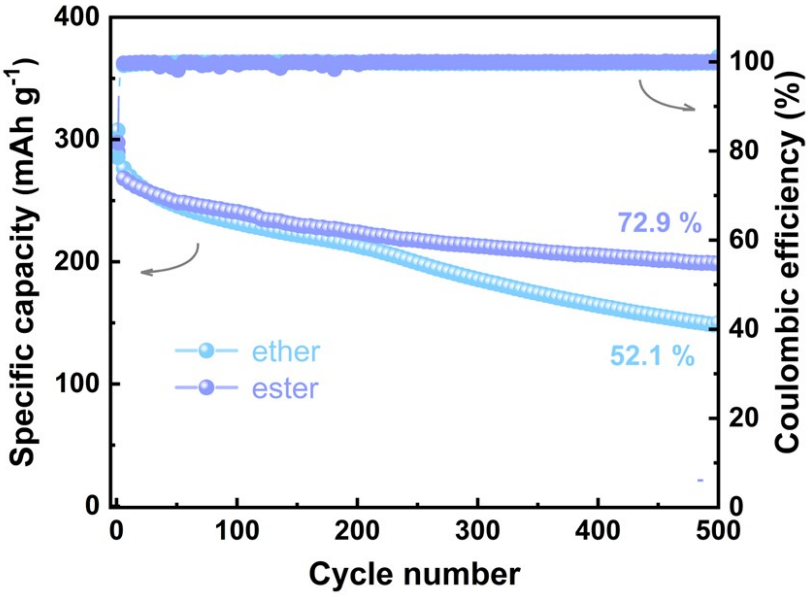

Fig. S26 Comparison of cycle performance of Prussian blue//HC-AL in ester-based and ether-based electrolyte.

Fig. S27 Paragraph for industrial production of HC-AL

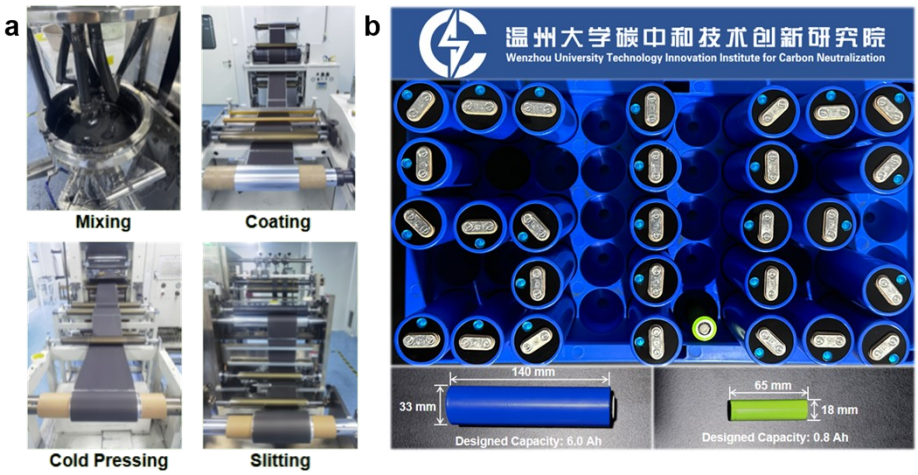

Fig. S28 (a) Paragraph for preparation process of HC-AL electrode, (b) Paragraph of 18650 type and 33140 type cylindrical batteries.

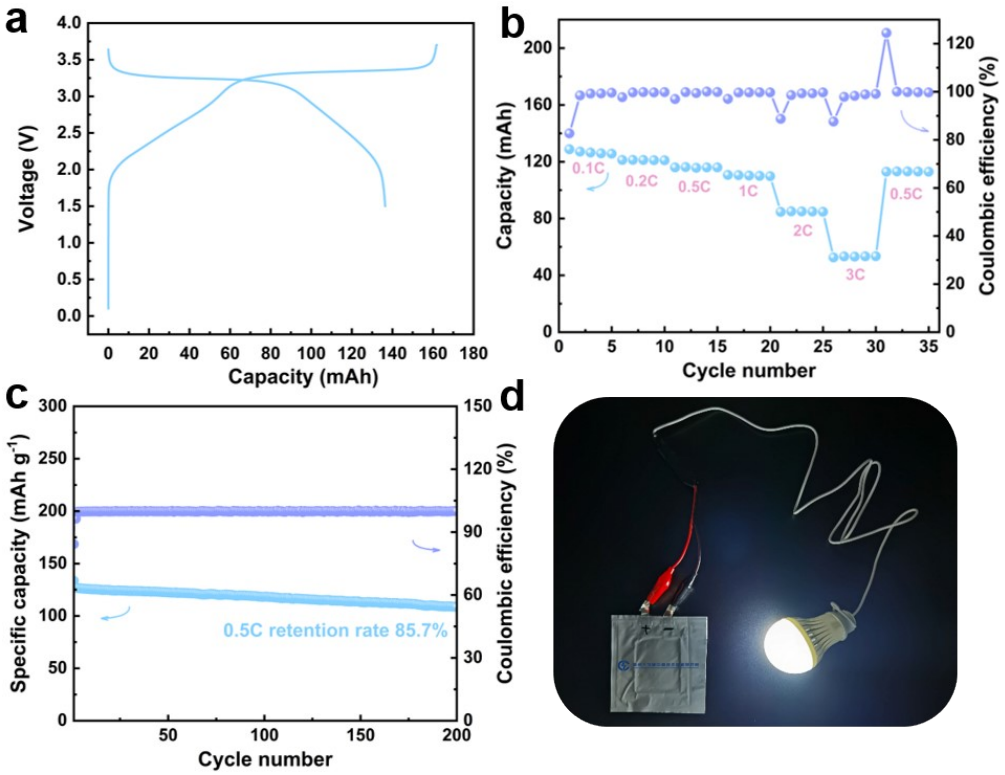

Fig. S29 (a) First charge/discharge curves, (b) Rate performance, (c) Cycle performance of Prussian blue//HC-AL pouch battery, (d) Photograph of lighting up a 3 V light bulb.

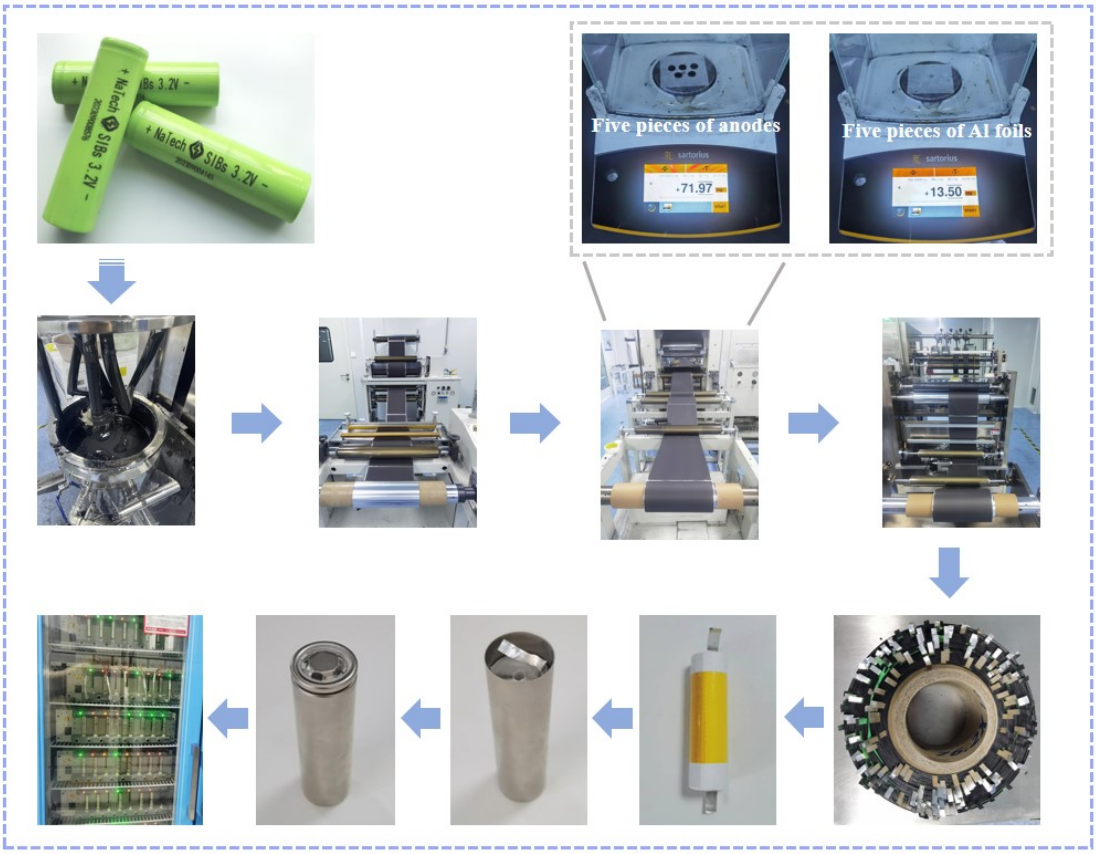

Fig. S30 Detailed preparation process of 18650 cylindrical battery.

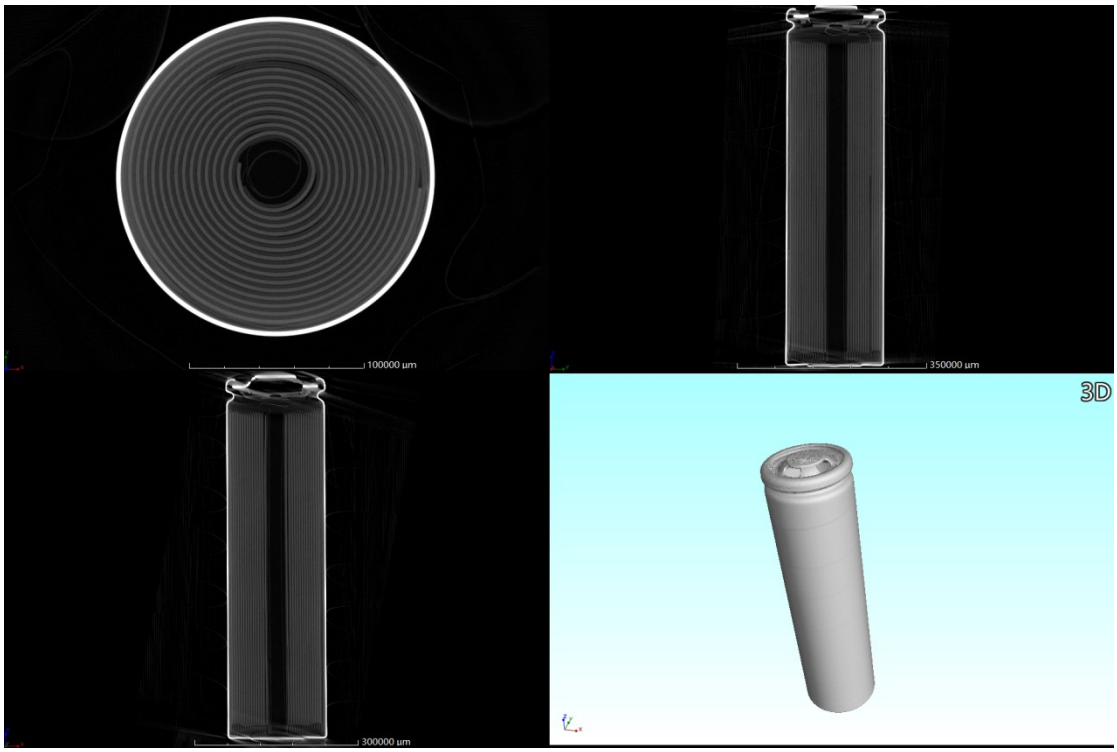

Fig. S31 Computed tomography picture of 18650 cylindrical battery.

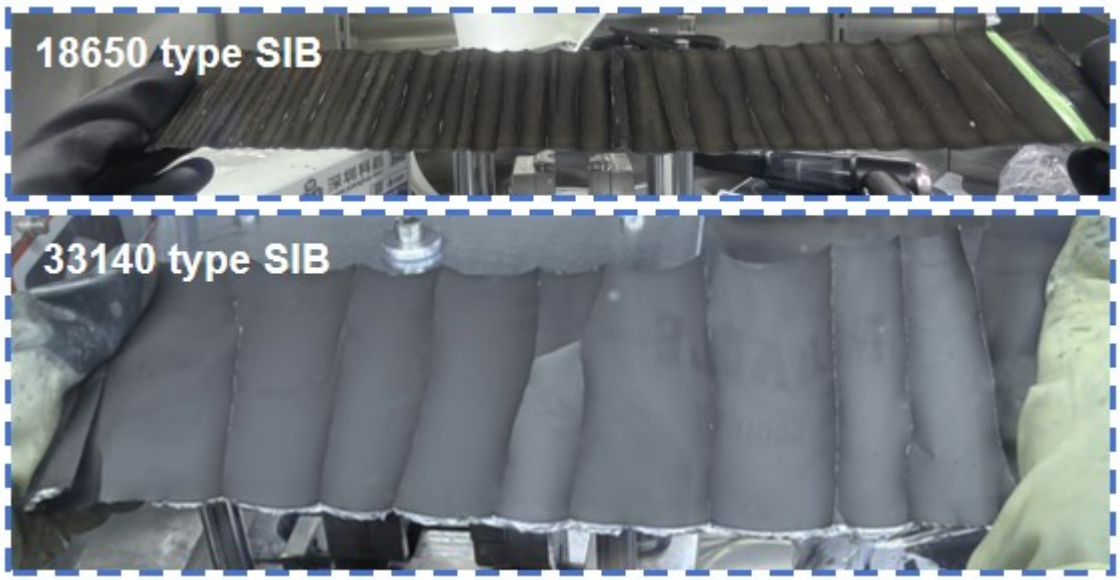

Fig. S32 The anode of unwrapped 18650 and 33140 type SIBs (the crease is caused by dismantling and tiling process of the electrode).

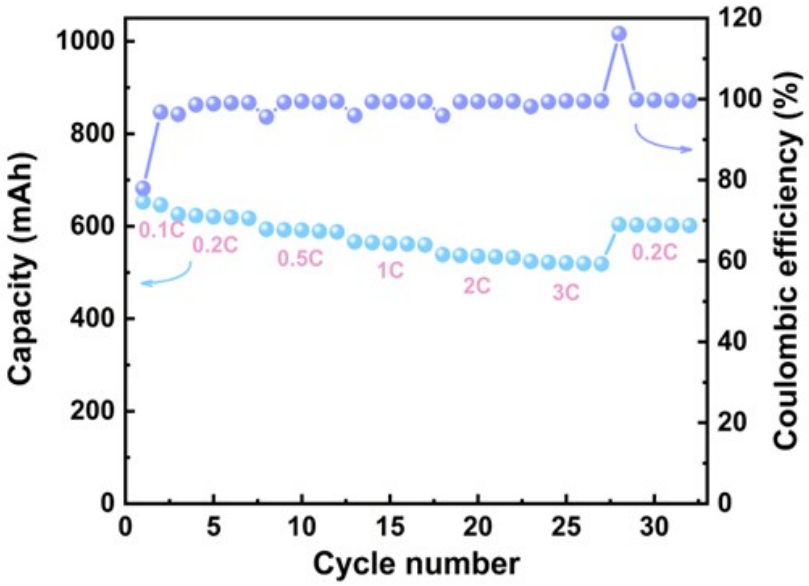

Fig. S33 rate performance of the 18650 batteries

Table S1 Physical parameters of the XRD spectra from hard carbon samples

	HC	HC-AL	HC-AM	HC-AH
Highly disordered	58%	55%	50%	44%
Pseudo-graphitic	41%	44%	49%	44%
Graphite-like	-	-	-	10%
2θ [°]	22.46/25.03	22.24/24.88	21.92/24.67	21.95/24.55/26.69
d_{002}	0.395/0.355	0.399/0.357	0.405/0.360	0.404/0.362/0.333
*L*c	1.63/2.12	1.82/2.06	1.78/1.871	1.90/2.11/8.078
FWHM	4.9/3.8	4.4/3.9	4.5/4.3	4.2/3.8/1.0
n	5.12/6.97	5.56/6.77	5.39/6.19	5.7/6.82/25.25

Table S2 Physical parameters of the Raman spectra from the samples

	AL	AM	AH	HC	HC-AL	HC-AM	HC-AH
A_{D4}/A_G	0.73	0.99	1.27	0.81	0.87	0.73	0.71
A_{D1}/A_G	1.53	1.38	1.77	1.67	1.84	1.65	1.66
A_{D3}/A_G	1.17	1.65	1.61	1.32	1.44	1.07	0.73

Table S3 The content of each element in the XPS spectrum and percentage of component after peak splitting fitting from O1s

	Percentage of element in the total spectrum (%)		Percentage of the component after peak splitting fitting (%)		
	C_{1s}	O_{1s}	-C-O	-C=O	-COOH
NL	72.51%	27.49%	89.5%	10.5%	-
AL	82.79%	17.21%	37.46%	49.63%	7.19%
AM	82.86%	17.14%	36.20%	50.35%	7.43%
AH	84.77%	15.23%	33.36%	54.43%	7.48%
HC	96.96%	3.04%	15.23%	79.81%	4.96%
HC-AL	96.15%	3.85%	14.66%	81.29%	4.06%
HC-AM	96.70%	3.30%	13.04%	83.58%	3.38%
HC-AH	96.99%	3.01%	14.44%	81.88%	3.68%

Table S4 Physical parameters from the gas absorption-desorption of the acid-treated bamboo, AL, AM and AH samples

	Specific surface area	N_2 adsorption-desorption	
	(m^2 g^{-1})	Pore volume (cm^3 g^{-1})	Diameter (nm)
Bamboo powder	1.505	0.005	2.187
AL	145.745	0.023	1.923
AM	282.725	0.048	1.918
AH	567.466	0.080	1.925

Table S5 Physical parameters from the gas absorption-desorption of the HC, HC-AL, HC-AM and HC-AH samples

	Specific surface area (m^2 g^{-1})	N_2 adsorption-desorption Pore volume (cm^3 g^{-1})	Diameter (nm)	CO_2 adsorption-desorption Pore volume (cm^3 g^{-1})	Diameter (nm)
HC	2.08	0.004	1.007	0.009	0.6
HC-AL	11.20	0.014	4.007	0.168	0.479
HC-AM	126.95	0.079	2.769	0.237	0.6
HC-AH	491.24	0.474	4.367	0.189	0.480

Table S6 Specific capacity of the samples on every sodium storage stages

		Specific capacity of adsorption (mAh g^{-1})	Specific capacity of pseudo-adsorption (mAh g^{-1})	Specific capacity of intercalation (mAh g^{-1})	Specific capacity of pore filling (mAh g^{-1})
Ester-based electrolyte	HC	91.82	50.28	127.15	80.85
	HC-AL	99.08	50.66	128.72	115.87
	HC-AM	126.48	50.81	113.42	130.47
	HC-AH	153.44	57.30	73.02	130.56
Ether-based electrolyte	HC	86.40	52.16	137.34	79.31
	HC-AL	88.88	50.35	145.52	117.03
	HC-AM	90.13	40.60	134.06	143.80
	HC-AH	86.74	43.49	124.58	159.80

Reference

1 P. E. Blöchl, *Phys. Rev. B.*, 1994, **50**, 17953-17979.

2 G. Kresse and J. Furthmüller, *Phys. Rev. B.*, 1996, **54**, 11169.

3 G. Kresse and J. Furthmüller, *Comp. Mater. Sci.*, 1996, **6**, 15-50.

4 G. Kresse and D. Joubert, *Phys. Rev. B.*, 1999, **59**, 1758.

5 J. P. Perdew, K. Burke and M. Ernzerhof, *Phys. Rev. Lett.*, 1996, **77**, 3865.

6 S. Grimme, J. Antony, S. Ehrlich and H. Krieg, *J. Chem Phys.*, 2010, **132**.